Validation of the Mars General Circulation Model and Climate Database with new spacecraft observations

François Forget, Yann Wanherdrick
(*Laboratoire de Météorologie Dynamique, Paris, France*)

Stephen R. Lewis
(*AOPP, Oxford University, UK*)

May 21, 2001
Technical note for ESA contract 11369/95/NL/JG,
Work Package 7

1 Introduction

This document describes a comparison of recent spacecraft observations of Mars with results predicted at similar locations and times in the Mars Climate Database (MCD) version 3.0. The Mars Climate Database V3.0 is a database of statistics directly compiled from a recent version of the LMD-AOPP General Circulation Model (GCM). Thus, this document can also be considered as an evaluation of the GCM.

Compared to previous versions, the new GCM and database cover a wider range of altitude, from 0 to 120 km in the vertical, they use improved topography and thermal inertia surface maps from Mars Global Surveyor (MGS), and include a new "dust scenario" to describe the distribution of airborne dust in the atmosphere also based on recent observations from MGS.

Most of the observations of Mars relevant for comparison with the climate database are measurements of the thermal structure of the atmosphere and its density. Of particular interest are the recent observations from Mars Global Surveyor. MGS reached Mars in september 1997. For the next 18 months its orbit was altered using the technique of aerobraking until it reached its so-called mapping phase in April 1999. One Martian year of mapping observations have thus been completed at the time of the writing of this report, although not all the observations are available yet.

Three kind of MGS observations are used in this report 1) Temperature profiles derived from radio-occultion of the MGS spacecraft by the Martian atmosphere 2) Temperature profiles derived by inverting the atmospheric thermal infrared emission as observed by the Thermal Emission Spectrometer 3) in-situ density measurement obtained in the upper atmosphere (120 km) during the aerobraking of MGS. In addition, (4) we also use here the in-situ temperature profiles measured by the three probes that have succesfully landed on Mars so far : Viking Lander 1 (1976), Viking Lander 2 (1976)

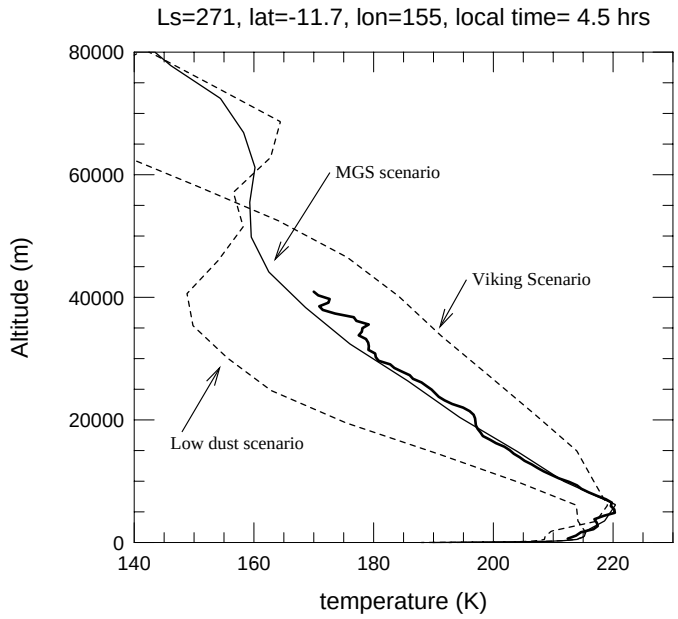

Figure 1: A typical temperature profile observed by radio-occultation (thick solid line, february 1998, $L_s = 271^o$, 11.7^oS-155^oE, local time : 4:30) compared to temperature profiles predicted by the database at the same time and location. Profiles from the "MGS" scenario were designed to be close to the MGS observations, whereas the "Viking" and "low dust" scenarios usually yield warmer and colder temperatures profiles in the lower atmosphere, respectively.

and Pathfinder (1997), as well as surface measurements from Pathfinder.

2 Comparison with Mars Global Surveyor Radio Occultations

The Radioscience instrument aboard MGS employs an ultra-stable radio oscillator. The signal from the oscillator to Earth is refracted by the Martian atmosphere, allowing retrieval of profiles of atmospheric density, pressure, and temperature versus radius and geopotential (Hinson et al., 1999, 2001).

Table 1 shows a list of the occultations available for this report for the various "seasons" of the Mars Climate database, with some general comments on the comparison MCD-observations. The data were separated in two kinds : on the one hand the occultations performed at sunlit latitudes (608 profiles), on the other hand occultations obtained in or near the southern winter polar night (491 profiles).

It must be noted here that the so-called "Mars Global Surveyor" dust scenario used as a reference in the database (See the "Mars Climate Database V3.0 Detailed Design Document) has been partly design to match the MGS observations, including the radio-occultations. As a result, the simulations performed with this scenario are generally close to the observations, whereas the "Viking" and "low dust" scenarios yield warmer

Sunlit atmosphere observations				
Season number	L_s (deg)	number of profiles	latitude (deg)	Comments
3	74. - 78.	36	64. - 67.	Spring polar atmosphere Good match, but MGS scenario 10K too warm at 30 km (very good match with low dust scenario)
4	111. - 115.	48	68. - 73.	Summer polar atmosphere. Very good match. Low atmosphere (0-5 km) slightly too warm (5-10 K). See Fig. 5.
5	134. - 149.	305	-6. - +36.	Often good match (especially above 20^oN) with discrepency due to waves. Around equator, large discrepency locally because of tides, gravity waves and/or clouds (Fig. 6).
6	150. - 161.	135	-30. - -6.	Good match but large discrepency locally because of tides, gravity waves and/or clouds.
9	264.-270.	8	-5. - +30.	Good (and often very good) match, with mall differences ($< 7\ K$) due to gravity waves and local dust distribution.
10	270. - 300.	65	-65. - -9.	Good (and often very good) match (see Fig 3) with mall differences ($< 9\ K$) mostly due to gravity waves and local dust distribution (Fig 4).
11	300. - 308.	11	-43. - -19.	Very similar structure but MCD profiles systematically about 10K colder due to dust distribution (Fig 4).

Polar night atmosphere observations				
Season number	L_s (deg)	number of profiles	latitude (deg)	Comments
4	111. - 115.	49	- 75.	see figure 7
5	134. - 150.	302	-69.5 - -66.8	idem
6	150. - 161.	140	-67.1 - -66.6	idem

Table 1: A list of the MGS radio-occultations temperature profiles available for this report binned into Mars Climate database “seasons”. The “Comments” column indicates the typical behavior of the GCM Mars Climate Database simulation when compared with observations at the same time and location.

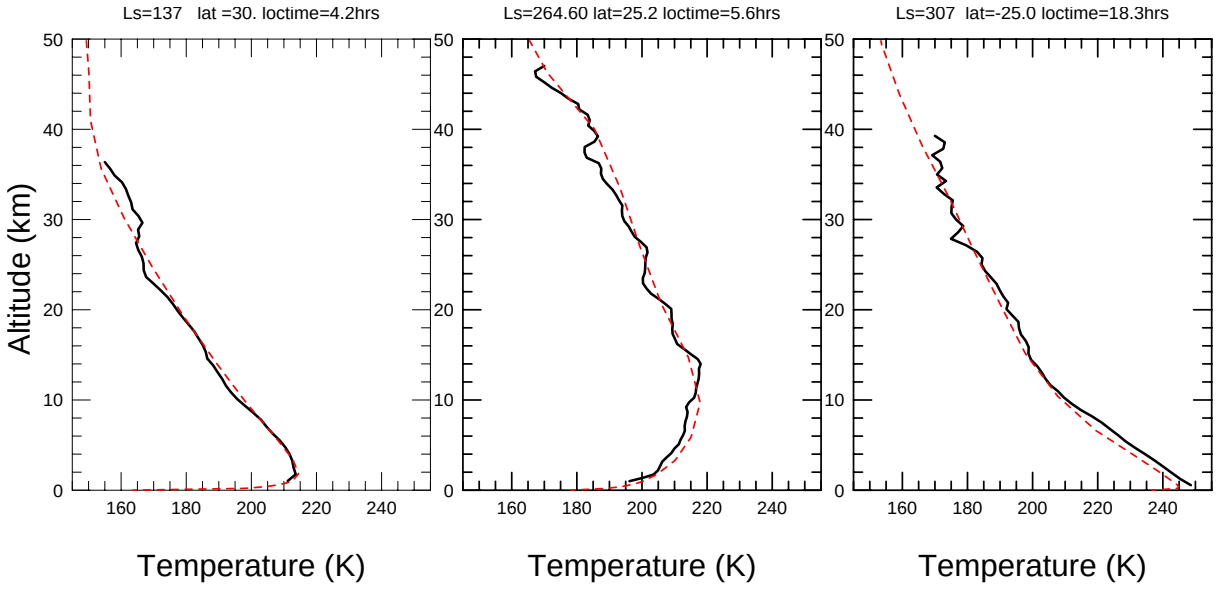

Figure 2: Example of very good fits to the observations that can be obtained with the database MGS scenario at various seasons in the tropics (Observation: black solid line ; Model: red dashed lines). Using this scenario, the model can usually well simulate the variations of the temperature profiles due to change in dust loading and insolation.

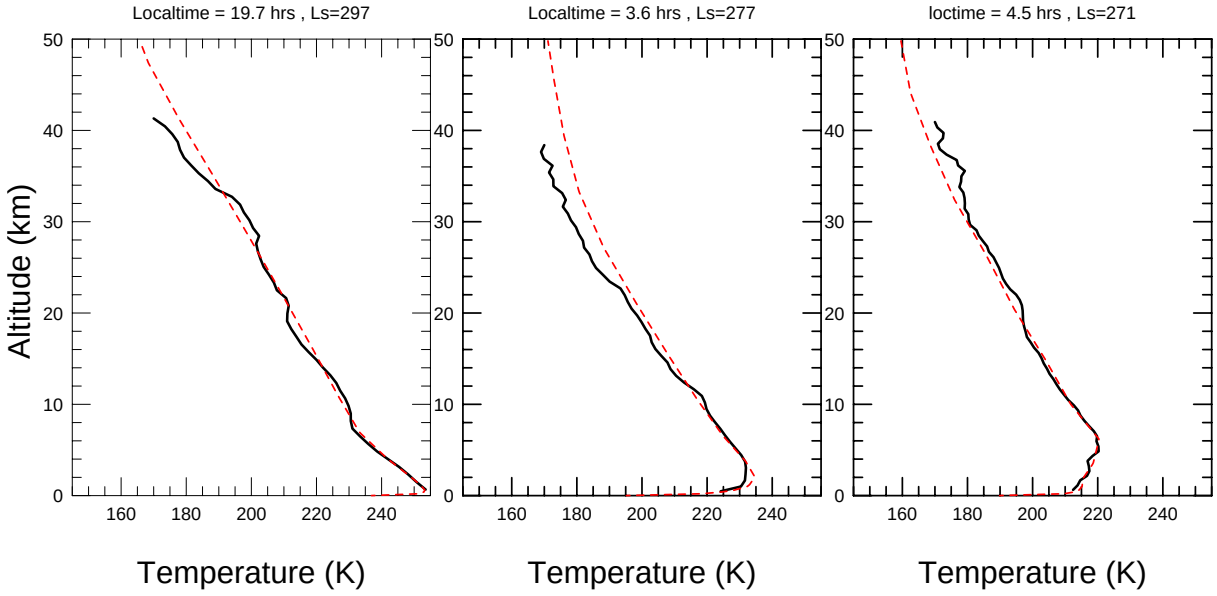

Figure 3: Example of very good fit of the observations that can be obtained in the lower atmosphere with the database MGS scenario at various local time (Observation: black solid line ; Model: red dashed lines) during summer in the southern hemisphere.

and colder temperatures profiles in the lower atmosphere, respectively (Figure 1). Below, we shall foccus on the comparison between the 'MGS" scenario database and the observations.

In general, very good agreement :

Using the MCD MGS scenario, the simulated temperature profiles are usually within 10K from the observations. Very often, the model is able to predict the detailed thermal structure of the atmosphere with a striking accuracy (Figure 2). This is true for various seasons and latitudes, corresponding to very different dust loading and insolation. This shows the ability of the model to simulate the impact of the duston the atmospheric thermal structure. Similarly, figure 3 illustrate the ability of the model to simulate the diurnal changes in the lower atmosphere thermal structure as a function of local time for 3 profiles, here obtained during summer in the southern hemisphere. In fact, for almost all the profiles obtained during southern summer (season 9,10,11), the low atmosphere thermal structure can amazingly be well reproduced by the model in spite of a large range of behavior. This is interesting: in their recent paper addressing the comparison of NASA Ames Mars GCM with this southern summer radioscience dataset, Joshi et al. (2000) noted that their model was not able to match such structures. For instance, unlike our model, the Ames GCM does not at all reproduce the temperature inversion peaking at 6 km shown on Figure 2, right (see Fig. 3 in Joshi et al. 2000), leading the Ames team to suggest that water ice clouds, an non-uniform vertical distribution of the dust or enhanced gravity wave activity was necessary to explain the observations.

Some problems, locally

Local variations in dust loading. During some seasons, the dust loading can be highly variable spatially and temporally. For instance, this is the case during summer in the southern hemisphere, leading to slight disagreement between observations and model, with modeled temperatures warmer or colder than the observations (Figure 4). However, the observed temperature profiles generally stay within the range covered by the "Viking" and "Low dust" scenario, except in major dust storms. In Fig 4, the profile predicted by the database at $L_s = 301^o$ (right) is quite colder than the observations. In this particular case, this also result from the fact that the database profile correspond to the average profile simulated for the period $L_s = 300 - 330^o$. During this period, the dust loading prescribed in the simulation quickly decrease. Thus, when compared with an actual profile obtained at the beginning of the period, it is not surprising to obtain relativy colder temperatures corresponding to a clearer atmosphere.

Low atmosphere in northern polar regions in summer. A small, systematic disagreement between the observations and the simulations of the low atmosphere thermal structure (< 5 km) is observed in the northern summer polar spectra (Figure 5). This could be due to non-realistic surface properties in the model (local ice) or to the impact of water ice clouds.

Waves and inversions in the Northern summer sub-tropics. Among the profiles observed during northern summer in the sub-tropics are found profiles containing suprisingly strong inversions (Figure 6). They are particularly found near pavonis Mons and Tharsis. These inversions are almost not reproduced by the model. Small "bumps" in the mean temperature profiles at altitude similar to the observed inversions can sometime be simulated, but the magnitude is much smaller than in reality (Figure 6). These inversions may results from dynamical phenomenons (tidal waves not well represented in the models, tidal waves interacting with subgrid-scale gravity waves) and/or the presence of water ice clouds. Water ice clouds are expected to create local inversions by radiatively cooling the atmosphere locally. The observed inversions are found where and when the thickest water ice clouds are observed on Mars. Their signatures is thus expected. However, it is unlikely that clouds can locally warm the profiles as it is often observed (e.g. bottom left profile in Figure 6).

Southern winter polar temperature. Figure 7 shows a subset of temperature profiles obtained around 70^oS latitude at various time during southern winter. Discrepencies between observations and models are obvious, especially toward the end of the winter when atmospheric temperature are getting warmer as the edge of the polar night receed toward the pole. Such differences are unexpected, although they may partly result from the fact that the database contains fields averaged over 30^o Solar Longitude. Further work is required to better understand the disagreement between model and observations.

3 Comparison with the The MGS Thermal Emission Spectrometer temperature retrieval

Infrared spectra returned by the Thermal Emission Spectrometer aboard MGS have been used for retrieval of the thermal structure of the Martian atmosphere (Conrath et al., 2000 ; Smith et al., 2001). Combined nadir- and limb-viewing spectra allow global monitoring of the atmosphere up to 0.01 mbar (65 km). Unfortunately, as we are writing this report, only temperature profiles retrieved from nadir spectra (and thus limited to the lower atmosphere) have been released to the science community in digital form. Nevertheless, three temperature cross-sections using both nadir and limb TES observations have been published by Smith et al. (2001), along with zonal wind field estimated by assuming gradient wind balance in the horizontal and hydrostatic balance in the vertical (note that gradient winds cannot be computed near the equator since the assumed force balance, i.e pressure gradient, Coriolis and centrifugal, is not valid at low latitudes). Figure 8, 9, 10 show such temperature and wind cross-sections at various seasons compared to zonal and time mean fields predicted by the database using the MGS dust scenario at the same seasons. A direct comparison is not straighforward. First, the TES retrievals correspond to a very low vertical resolution since the weighting function are very broad (see Conrath et al. 2000). As a result, the TES thermal structure may appear artificially "isothermal" between 1 and 0.1 mbar and near the surface. Second, the Climate Database plots are true zonal and time means (over a $30^o L_s$ interval) whereas the TES plots mainly combine observation at 2am and

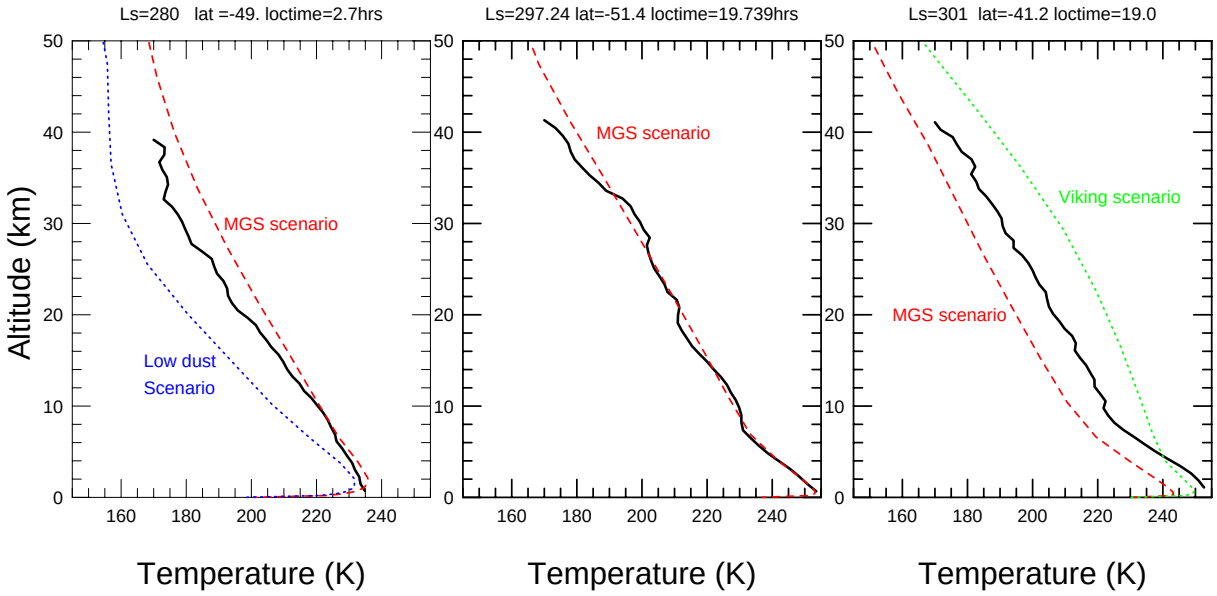

Figure 4: Examples of radio-science temperature profiles (solid, black lines) obtained during summer in the southern hemisphere. The actual dust loading seems to vary a lot in space and time, leading to small discrepency when compared to the Climate database predictions (red dashed lines) which used a more uniform dust loading. The observed temperature profiles stays within the range covered by the "Viking" (green) and "Low dust" (blue) scenarios.

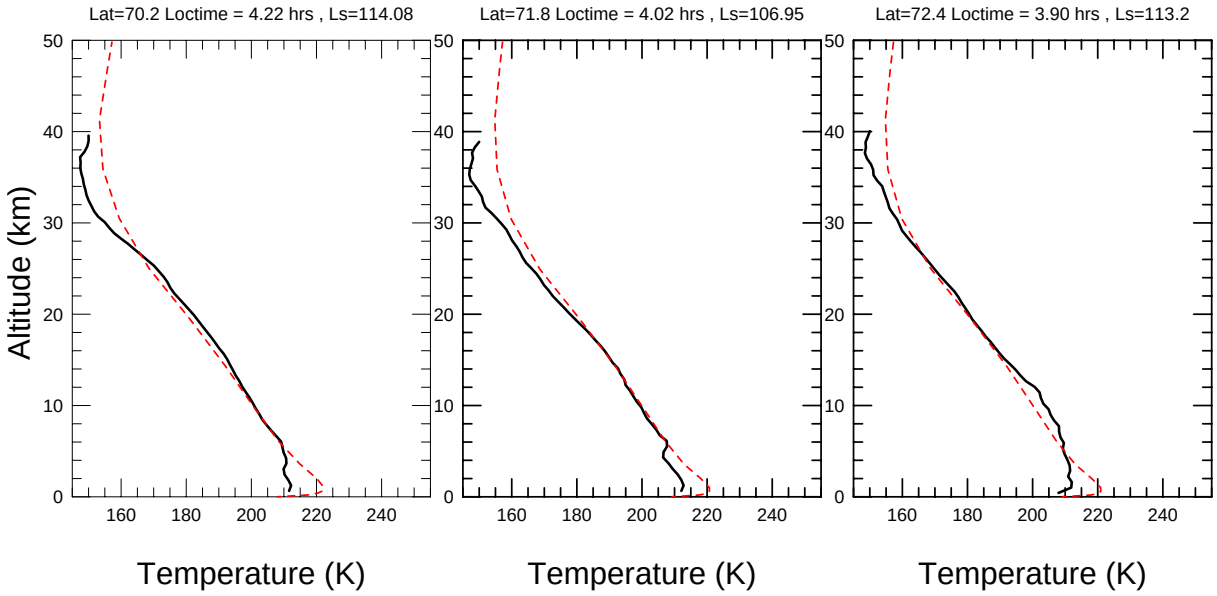

Figure 5: Examples of temperature profile comparison (Observations: black solid line ; MCD: red dashed lines) in the North Polar region in summer. Note the systematic disagreement observed in the low atmosphere.

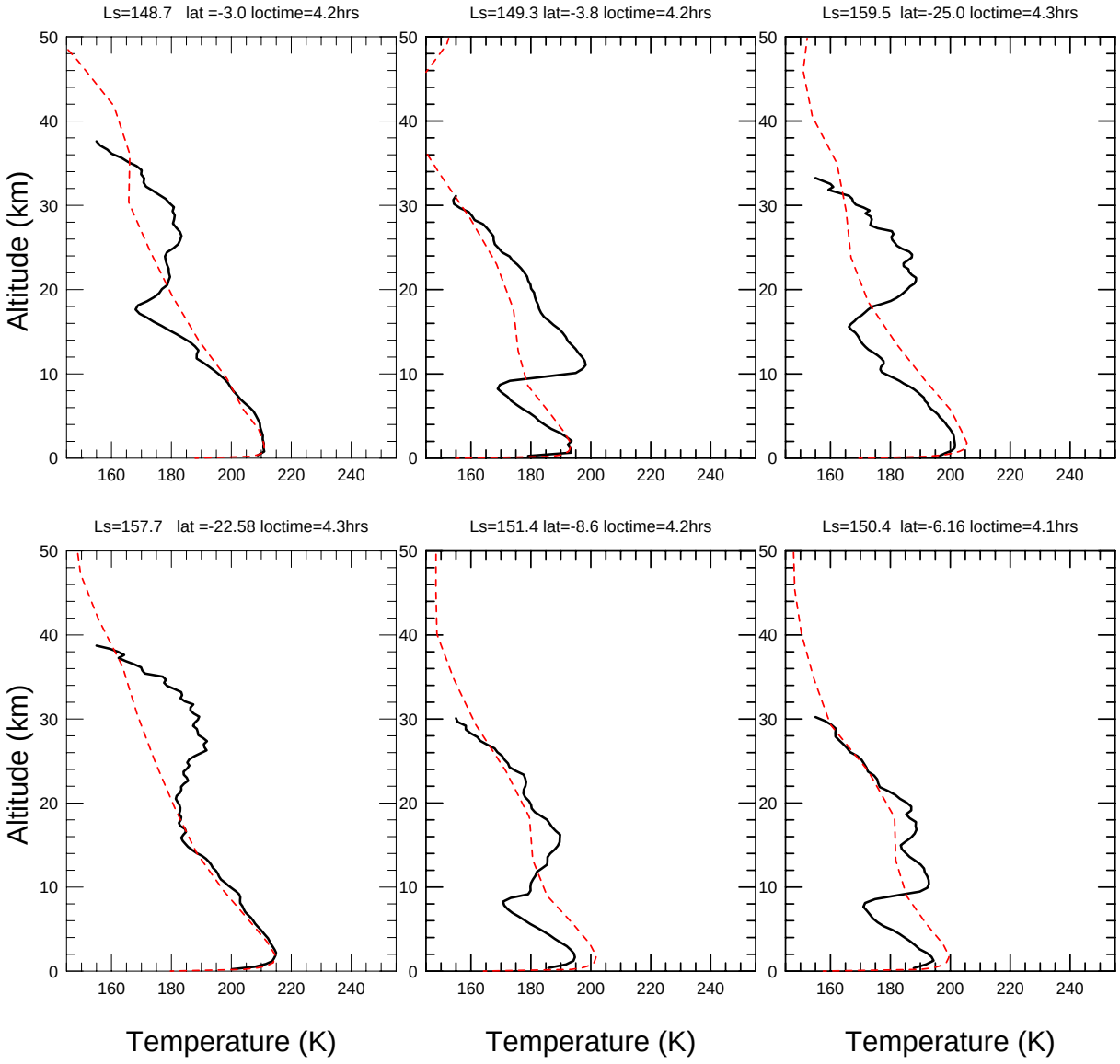

Figure 6: Six examples of radioscience profiles (solid black lines) from the northern summer tropics exhibiting strong temperature inversions which are not reproduced by the Mars Climate Database Prediction (red dashed lines).

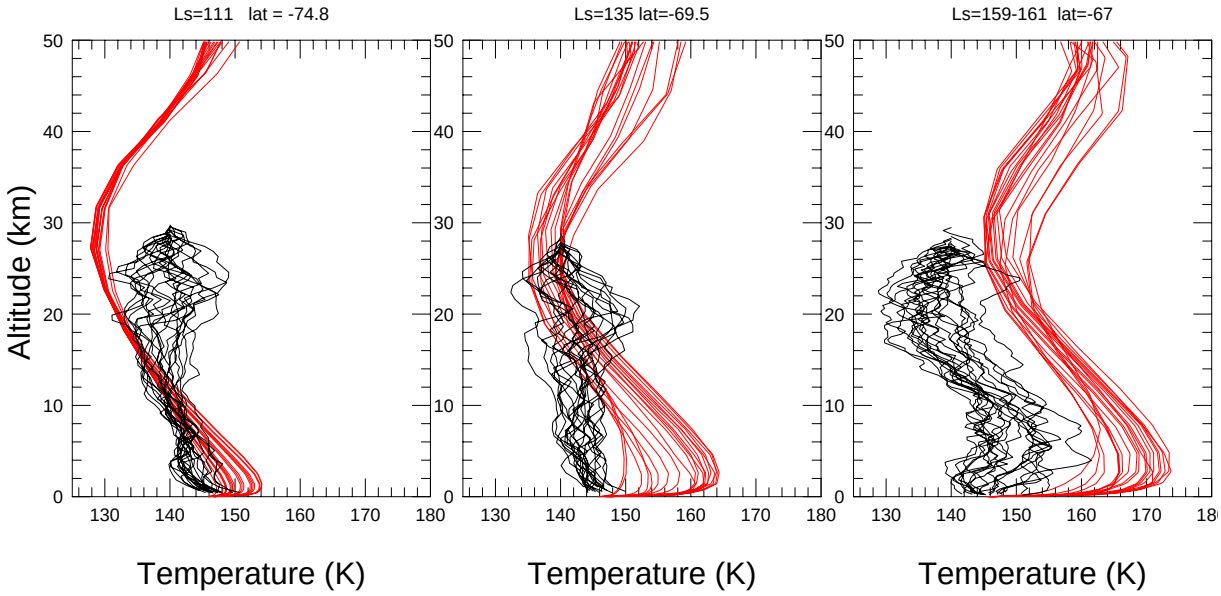

Figure 7: Three sets of 20 radio-science profiles (black) obtained in the south polar region in or near the polar night at different date, compared to sets of Mars Climate Database predictions (red) at the same time and location.

2pm, with a possible bias toward 2am or 2pm. Within this context, the model results apears to be relatively consistent with the observations. In particular, the mean temperatures would match well if one box-average them on a scale height as the retrieval processes actually does. One can notice that the simulated summer pole atmosphere at $L_s = 270^o$ is slightly cooler than in the TES inversions, resulting in weaker or absent simulated easterly winds high in the summer hemisphere. This discrepency is probably due to the occurence of a regional dust storm between $L_s = 260^o$ and $L_s = 272^o$ at the edge of the south polar cap during the year observed by MGS (Smith et al. 2001, plate 3).

4 Comparison with lander entry profiles

Figure 11 shows temperature measurement taken during the entry phases of the Viking landers (Seiff and Kirk, 1977) and Pathfinder (Magalhães et al., 1999) compared with MCD prediction at the same location and time for the MGS and Viking Scenarios. In the lower atmospere below 40 km, the three temperature profiles are at least 10 K warmer than our “best guess” MGS scenario. They are better matched by the Viking scenario, although for Viking 1 this is still not warm enough. These results are surprising since the Viking scenario profiles are almost always warmer than the radio-occultation profiles obtained at similar location and time. Could this be due to interranual variability ? In fact, the entry profiles appear more and more to be in conflict with remote observations obtained simultaneously (Clancy et al., 2000, Dave Hinson, personnal communication, 2001). This could be due to local effects and/or to some misunderstanding in the data analysis.

TES data and MGS scenario at $L_S = 135°$

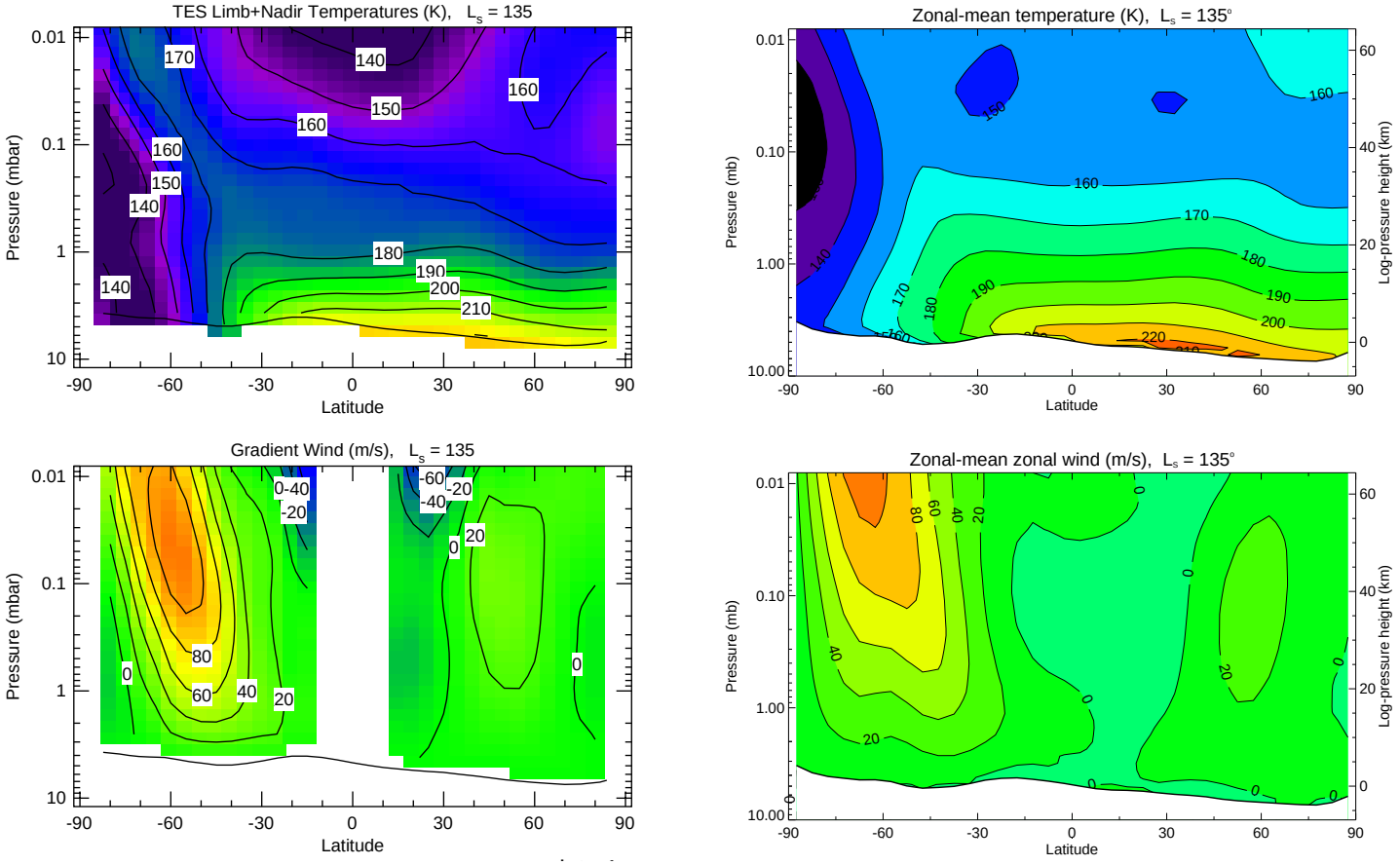

Figure 8: Mean meridional cross-sections of TES retrieved atmospheric temperatures (top, left pannel) and gradient winds (bottom, left pannel) at $L_s = 135^o$ compared to time-mean zonal-mean plots from the Mars Climate database using the MGS scenario for the same season. TES figure from Smith et al. (2001).

TES data and MGS scenario at $L_S = 180°$

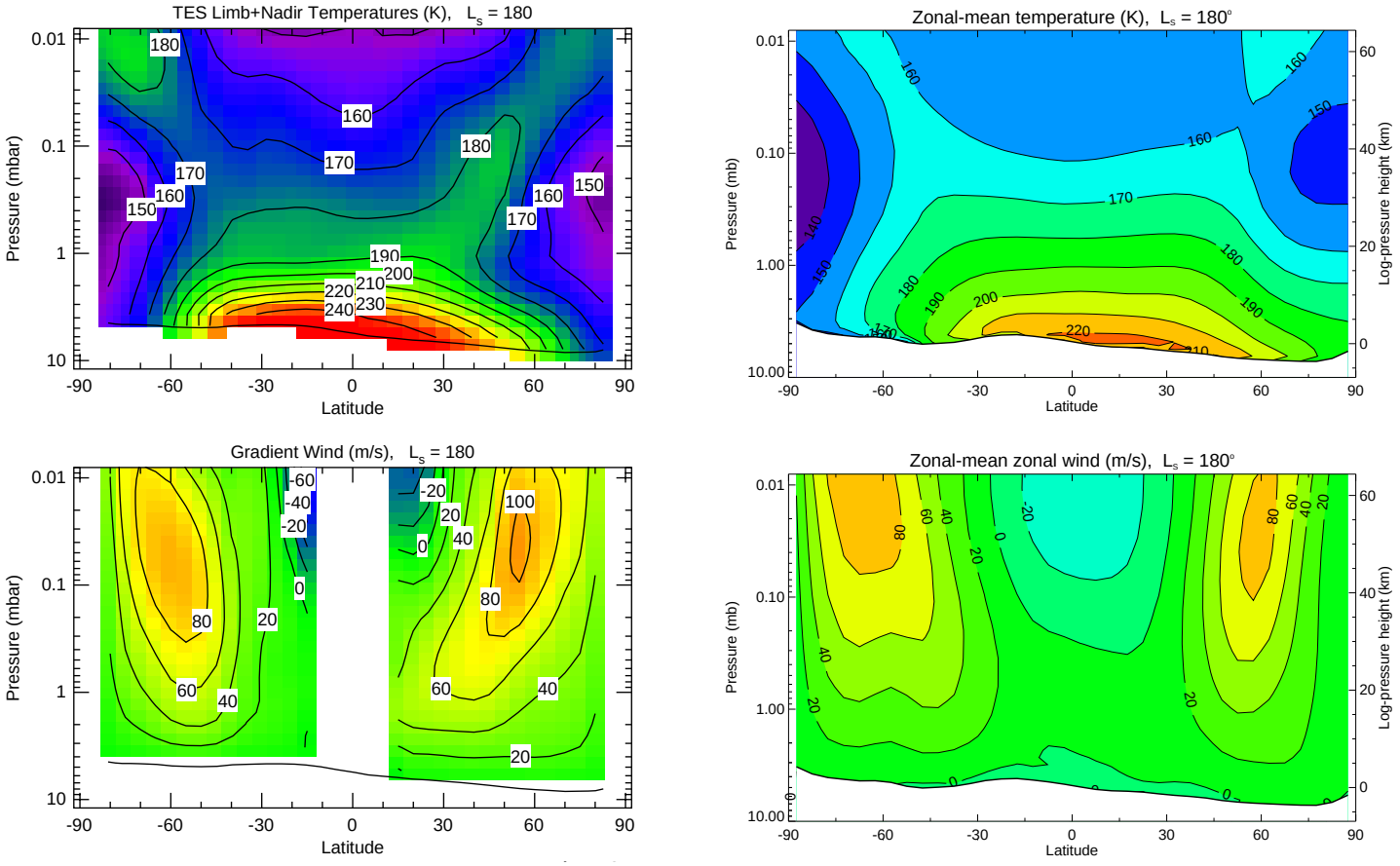

Figure 9: Same as figure 8 around $L_s = 180^o$

TES data and MGS scenario at $L_S = 270°$

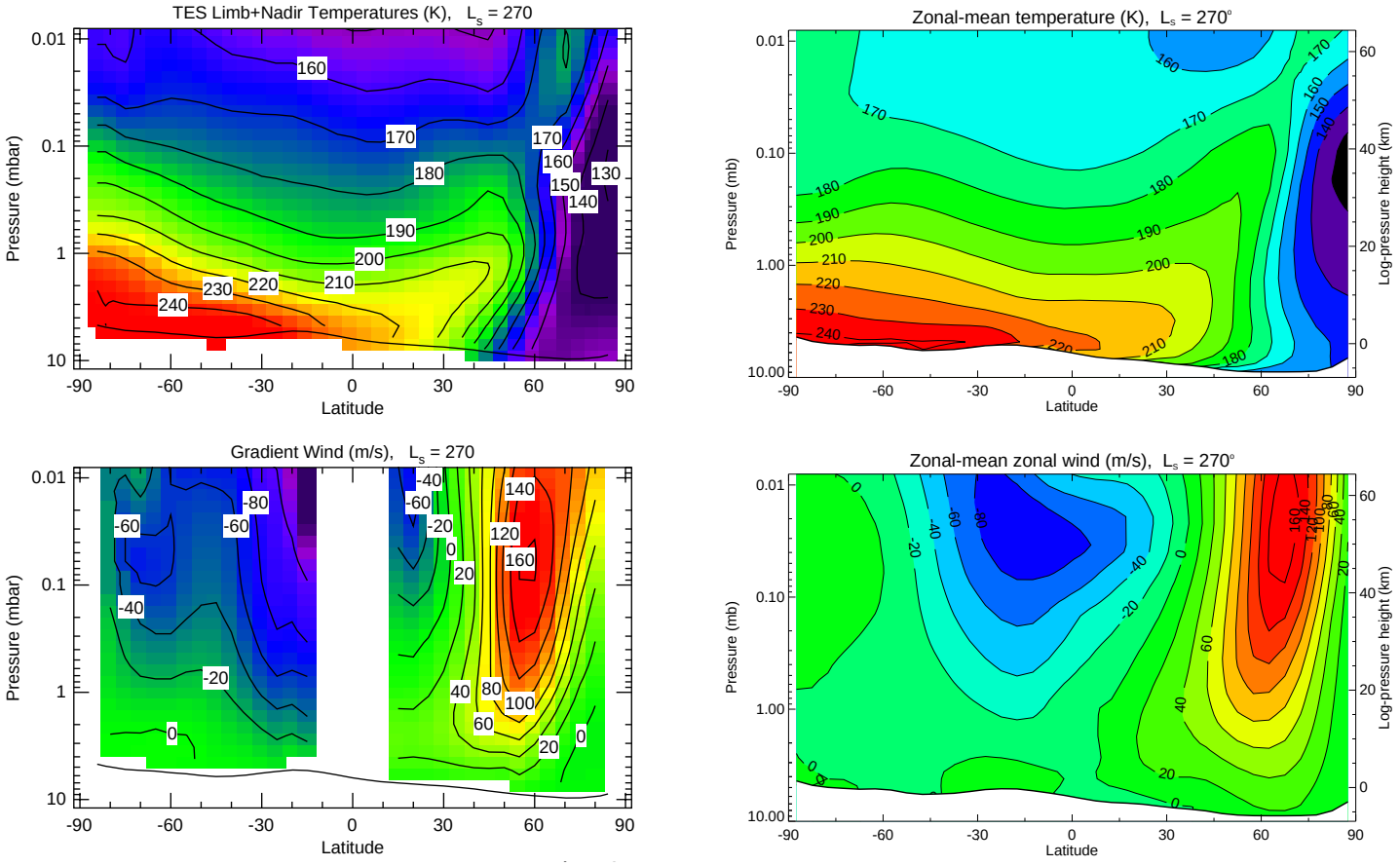

Figure 10: Same as figure 8 around $L_s = 270^o$

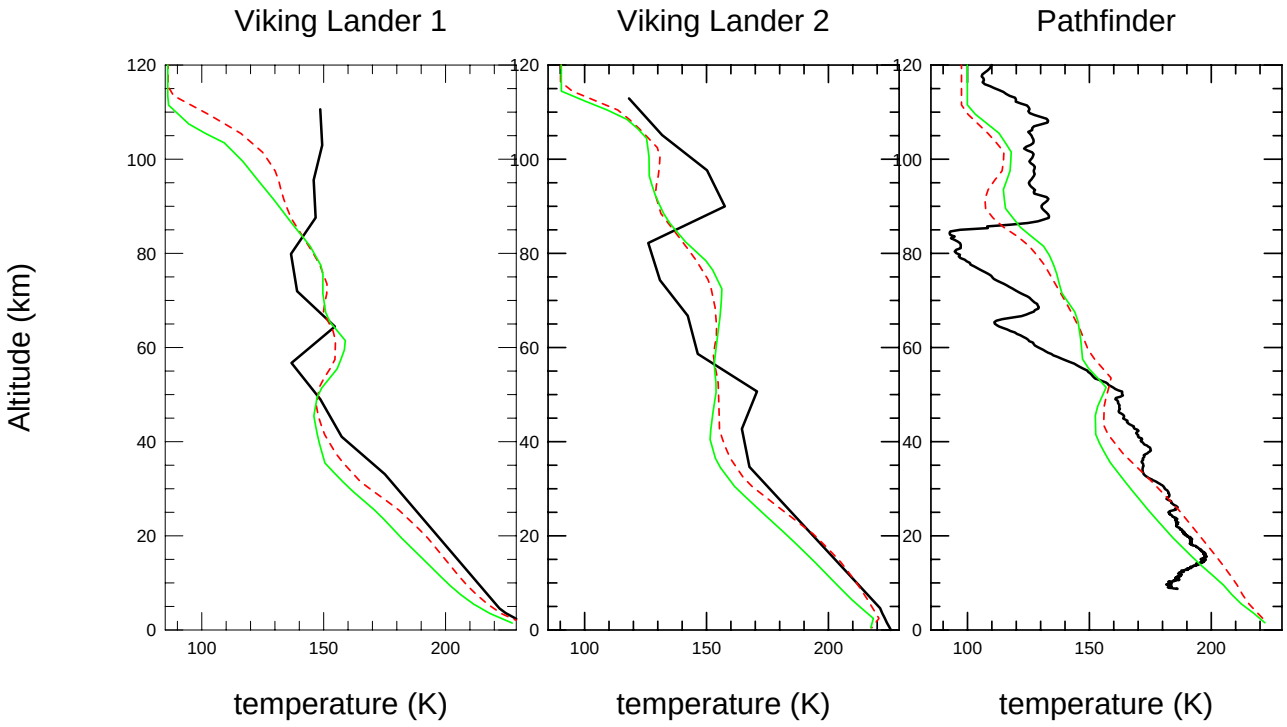

Figure 11: Entry Temperature profile (thick black line) observed in situ by the Viking and Pathfinder landers compared with GCM profiles retrieved from the Mars Climate database MGS scenario (green solid line) and Viking scenario (red dashed line).

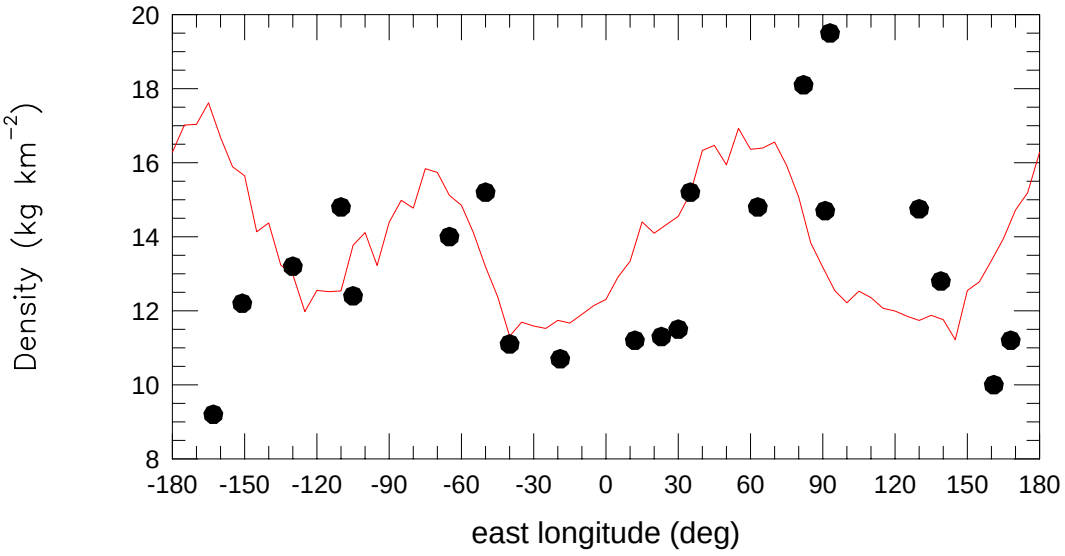

Figure 12: Observed longitudinal variations of the atmosphere density (red dots) normalized to 125 km above the DTM areoid by Mars Global Surveyor during the first Aerocapture phase (Keating et al., 1998) compared to prediction from the climate database (MGS scenario) in similar conditions ($Ls = 240^o$, local time : 13:00, latitude: 35^oN, 123 km above the MOLA areoid).

5 Comparison with upper atmosphere density aerobraking measurements

Figure 12 show a comparison of the density measured in-situ by the Mars Global Surveyor accelerometer during aerobraking around 125 km during northern winter (Keating et al., 1998) with the densities predicted at about the same location by the Mars Climate Database. A very good agreement is found, for two reasons : 1) on the one hand, the absolute value of the density is very well predicted in spite of the extreme sensitivity of density to the entire atmosphere below. 2) the Mars Climate database predict longitudinal variations comprising wave-like wavenumber 1 and 2 structures which are quite similar to the observations. This observed structure has been interpreted as the signature of nonmigrating tides which owe their existence to Mars' topography (Forbes and Hagan, 2000).

Very little MGS accelerometer measurements of the high Martian atmosphere has been published so far, but we know that a larger dataset has been obtained (J. Keating, private communication). In the future, it will be very interesting to compare other measurements (e.g. obtained during dust storms) with database predictions.

6 Comparison with Pathfinder surface observations.

The Atmospheric Structure Investigation/Meteorology experiment on the Mars Pathfinder spacecraft (Schofield et al., 1997) provides high temporal resolution near surface data

from the summer tropics (19^{o}N, 33^{o}W, starting at $L_s = 142^o$). In particular, observations of surface pressure, temperature, and wind direction over the primary 30 day phase of the mission allow the MCD representation of the diurnal cycle to be tested in some detail. Both the observations and the MCD indicate very little nondiurnal variability, other than the seasonal trend, at the Pathfinder site at the time of year at which the mission landed ($L_S = 142^o$); however, the diurnal cycle is strong.

The seasonal mean surface pressure cycle is compared with Pathfinder data in Figure 13 and can be seen to be in good agreement with the observations. For most scenario, the phase of the diurnal and semidiurnal tides is very well predicted. The amplitude is sensitive to the dust scenario. Interestingly, the MGS scenario appears to underestimate the total amplitude of the surface pressure tide, whereas the Viking dust scenario appears to give a better fit. Figure 14 shows the temperature on the Pathfinder meteorological mast compared with MCD predictions, and Figure 15 shows the wind direction; unfortunately, the wind amplitude is still not well calibrated in the observations at this stage and cannot be compared. In each case the MCD prediction is relatively good, especially considering the spatial resolution of the database and the comparison with a single point observation. It is therefore possible to have confidence in the representation of the diurnal cycle in the MCD, at least in as far as it is possible to test it at this stage.

7 Conclusion

Although the Mars Climate Database (MCD) version 3.0 was compiled from the results of General Circulation model experiments rather than directly from empirical fits to observational data, the MCD appears to be consistent with most of the available observational data for the atmosphere of Mars currently available. The present document only provides a limited number of comparison. In the future, we shall continue this validation processes with the new MGS data that are only starting to be fully available. Nevertheless, this report motivates future enhancement and extension of the GCM. In particular, reproducing the details of the observed variations of the thermal structure probably requires the full simulation of the dust cycle and the inclusion of water ice aerosols. Also, we are working on the direct assimilation of the temperature observations into the GCM, as in terrestrial meteorology and numerical weather prediction.

8 Appendix : update of the GCM surface thermal inertia map using the Mars Gobal Surveyor TES data

New thermal inertia data was provided by Mike Mellon (Mellon et al., 2000) from the University of Colorado, Boulder. It has allowed us to create a new thermal Inertia map, suitable for Climate modelling, which has been used to produce the Mars Climate Database V3.0.

This new dataset originates from the Mars Global Surveyor Thermal Emission Spectrometer. At the time of the studies, the available TES data did not allow to retrieve

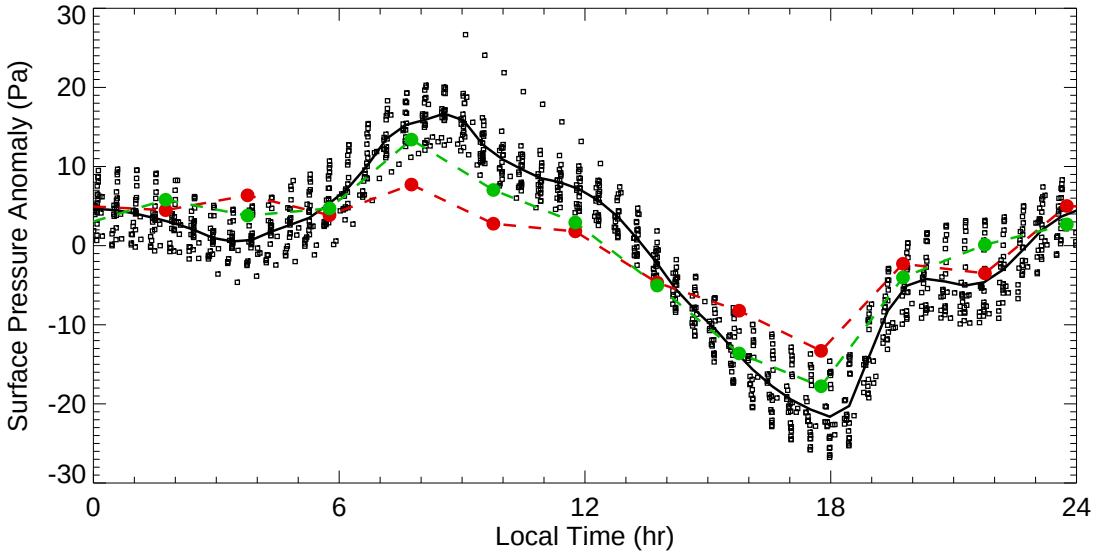

Figure 13: A comparison of the Mars Pathfinder surface pressure diurnal cycle with the MCD. The small squares show the Mars Pathfinder pressure measurements, taken 51 times per day, and the solid line is the mean of the observations taken over the first 30 days of the mission. The large circles connected by dashed lines show the MCD mean surface pressure interpolated to the Mars Pathfinder location. The red line is for the MGS scenario (the low dust scenario gives very similar results) and the green line for the Viking scenario. In this case the MGS scenario appears to underestimate the total amplitude of the surface pressure tide, whereas the Viking dust scenario appears to give a better fit. In both cases the diurnal-mean surface pressure has been subtracted.

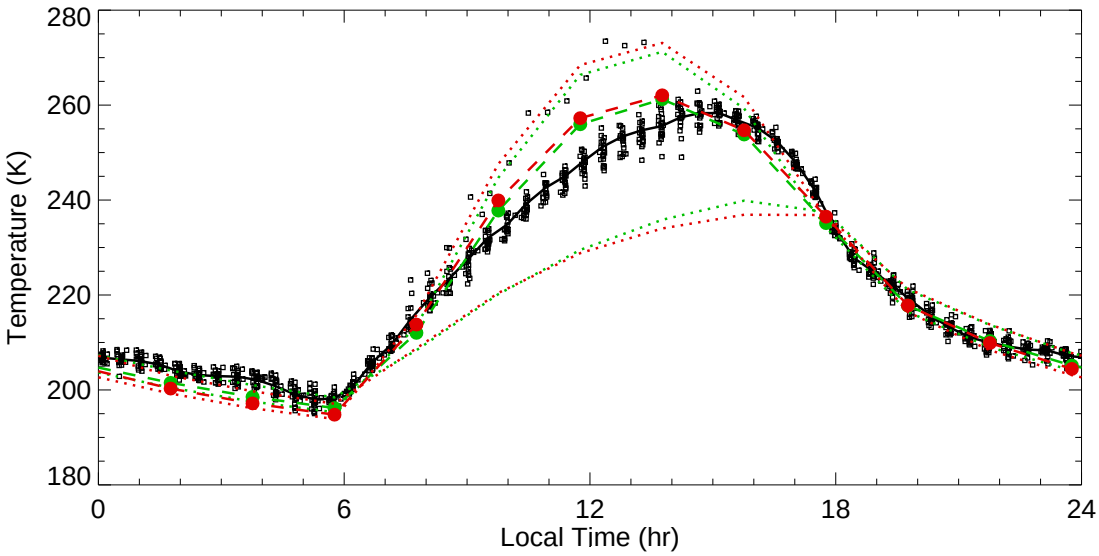

Figure 14: A comparison of the Mars Pathfinder temperature at the top of the 1 m meteorological mast (about 1.27 m above the Martian surface) with the MCD. As in Figure 13, the small squares show the individual measurements, and the solid line is the mean over 30 days. The dotted lines are the MCD surface temperature (top line at midday) and the MCD lowest atmospheric level temperature (bottom line) which is at a height of almost 5 m. The large circles connected by dashed lines show a linear interpolate between the two at a height corresponding to the top of the Pathfinder mast for a rough comparison (a linear interpolate might not be strictly appropriate in the unstable boundary layer). As in Figure 13, the red line is for the MGS scenario and the green line for the Viking scenario. The near-surface temperatures are not sensitive to moderate dust loadings.

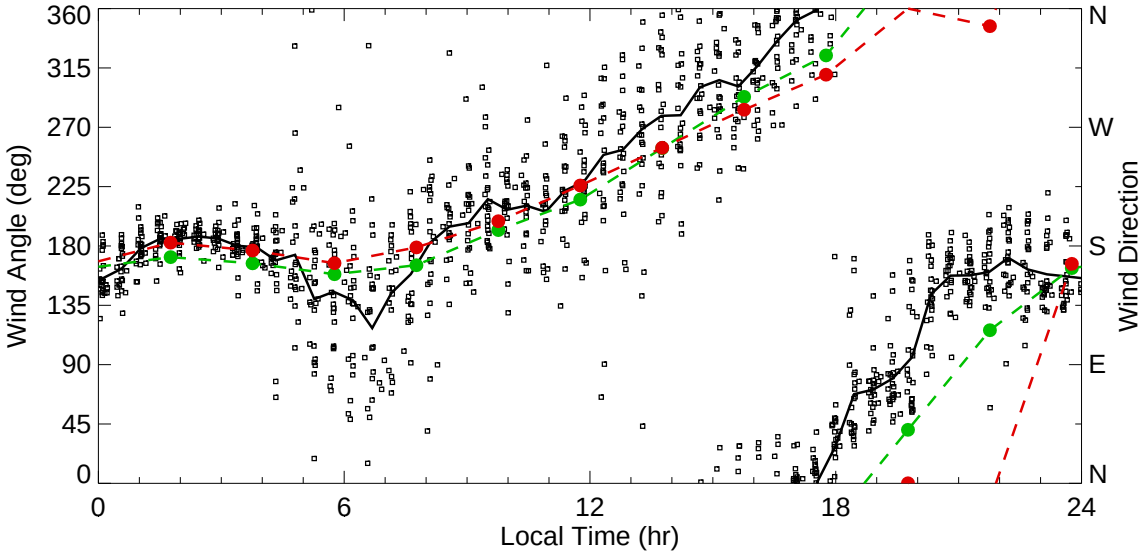

Figure 15: A comparison of the Mars Pathfinder wind direction with that at the lowest atmospheric layer in the MCD. As in Figure 13, the small squares show the individual measurements, and the solid line is the mean over 30 days. The large circles connected by dashed lines show the mean wind direction from the same point in the MCD; again, the red line is for the MGS scenario and the green line for the Viking scenario. The wind direction axis indicates the compass point which the wind is blowing from; a wind angle of 0° is a northerly. The general sense of rotation is determined by the passage of the diurnal thermal tide; the details, such as the small rotation toward an easterly near dawn before the subsequent rotation to a westerly, are a consequence of the local topography. As in Figure 14 the broad agreement is not sensitive to details of the dust scenario, though there is some evidence of better agreement with the Viking scenario in the evening.

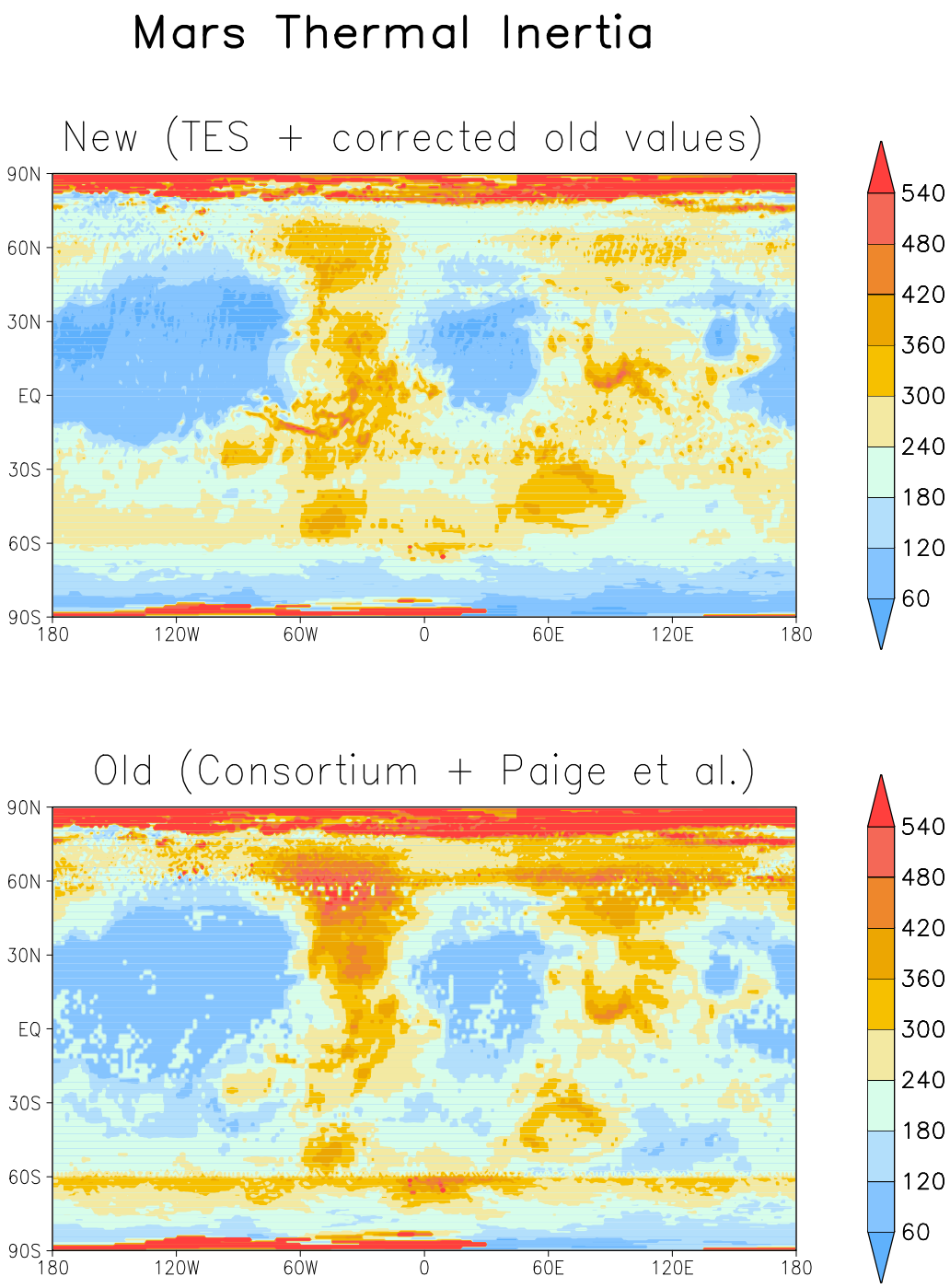

Figure 16: The new $1^o \times 1^o$ map of thermal inertia (J m^{-2} $s^{-1/2}$ K^{-1}) deduced from the new TES observations compared to the previous map (bottom) used for the GCM.

thermal inertia for latitude higer than 65^{o}North and 60^{o}South. Besides, the data obtained south of 30^{o}South were clearly suspicious, probably because they were obtained during winter time. Therefore, we decided to use only new TES data obtained between 65^{o}North and 30^{o}South.

For the rest of the map we continue to use the canonic thermal inertia map from Palluconi and Kieffer (1981) extended to the polar region using the more recent result from Paige et al. (1994) and Paige and Keegan (1994). However, on the basis of the analyses performed by Haberle and Jakosky (1991) and Hayashi et al. (1995) regarding the impact of the airborne dust on thermal inertia (not properly accounted in these less recent analyses), we applied some correction to the old dataset. Overall, the new thermal inertia map is built with the following components :

- **Between 90^{o}N and 65^{o}N:** We use the data from Paige et al. (1994) available between 90^{o}N and 60^{o}N:. In their analyses, these authors simply neglected the dust in the atmosphere. On the basis of the studies mentionned above and after comparing the Paige et al. (1994) with the new TES data where both data are available between 60 and 65^{o}N, the Paige et al. (1994) were decreased by 25%.

- **Between 65^{o}N and 60^{o}N:** Linear transition (weighted averaging) between the corrected Paige et al. (1994) data with the TES data. In practice, there are not any big differences between the two datasets, but we have preferred to smooth all the same.

- **Between 60^{o}N and 30^{o}S:** new TES data

- **Between 30^{o}S and 60^{o}S:** Palluconi and Kieffer (1981) data, decreased by 8%. This correction was found to insure a smooth transition between the TES data and the old data. The correction is lower than the mean planetary value suggested by Hayashi et al. [1995] (20% decrease). This is probably due to the fact that this latitude belt is mostly composed of highlands. In such high altitude regions, the total airmass above the ground, and thus the total dust column, is lower than average. Thus, the correction for dust can be only 8% rather than 20%.

- **Between 60^{o}S and 90^{o}S:** Corrected Paige and Keegan (1994). Here also, these authors did neglect the impact of the airbone dust on the retrieved thermal inertia. Althought this area is also composed of highlands, the dust loading in this part of the planet was probably quite high in the Viking IRTM dataset used for the retrieval since these were obtained at the end of the dusty season ($L_s = 321 - 338^o$). On this basis, and because the comparison with the Palluconi and Kieffer (1981) data around 60^{o}S showed that the Paige and Keegan (1994) data are much below the Palluconi and Kieffer (1981) data (see figure 11 in Paige and Keegan, 1994) which themselves were shown to be underestimated by Hayashi et al., we have decreased the Paige and Keegan (1994) data by 28%. This allow a smooth transition between the corrected Palluconi and Kieffer (1981) data with the corrected Paige and Keegan (1994).

References

[Clancy et al., 2000] Clancy, R. T., Sandor, B. J., Woff, M. J., Christensen, P. R., Smith, M. D., Pearl, J. C., Conrath, B. J., and Wilson, R. J. (2000). An intercomparison of ground-based millimeter, MGS TES, and Viking atmospheric temperature measurements: Seasonal and interannual variability of temperatures and dust loading in the global Mars atmosphere. *J. Geophys. Res.*, 105:9553–9571.

[Conrath et al., 2000] Conrath, B. J., Pearl, J. C., Smith, M. D., Maguire, W. C., Christensen, P. R., Dason, S., and Kaelberer, M. S. (2000). Mars Global Surveyor Thermal Emission Spectrometer (Tes) observations : atmospheric temperature during aerobraking and science phasing. *J. Geophys. Res.*, 105:9509–9519.

[Forbes and Hagan, 2000] Forbes, J. M. and Hagan, M. E. (2000). Diurnal Kelvin wave in the atmosphere of Mars: Toward and understanding of "Stationary" density structures observed by the MGS accelerometer. *Geophys. Res. Lett.*, 27:3563–3566.

[Haberle and Jakosky, 1991] Haberle, R. M. and Jakosky, B. M. (1991). Atmospheric effects on the remote determination of thermal inertia of Mars. *Icarus*, 90:187–204.

[Hayashi et al., 1995] Hayashi, J. N., Jakosky, B. M., and Haberle, R. M. (1995). Atmospheric effects on the mapping of Martian thermal inertia and thermally derived albedo. *J. Geophys. Res.*, 100:5277–5284.

[Hinson et al., 1999] Hinson, D. P., Flasar, M., Simpson, R. A., Twicken, J. D., and Tyler, G. L. (1999). Initial results from radio occultation measurements with mars global surveyor. *J. Geophys. Res.*, 104:26,997–27,012.

[Hinson et al., 2001] Hinson, D. P., Tyler, G. L., Hollingsworth, J. L., and Wilson, R. J. (2001). Radio occultation measurements of forced atmospheric waves on Mars. *J. Geophys. Res.*, 106:1463–1480.

[Joshi et al., 2000] Joshi, M., Haberle, R. M., Hollingsworth, J., and Hinson, D. (2000). A comparison of MGS phase 1 aerobraking radio occultation data and the NASA Ames Mars GCM. *J. Geophys. Res.*, 105:17,601–17615.

[Keating et al., 1998] Keating, G. M., W., B. S., and 29-coauthors. (1998). The structure of the upper atmosphere of mars: In situ accelerometer measurements from Mars Global Surveyor. *Science*, 279:1672–1676.

[Magalhães et al., 1999] Magalhães, J. A., Schofield, J. T., and Seiff, A. (1999). Results of the Mars Pathfinder atmospheric structure investigation. *J. Geophys. Res.*, 1999:8943–8956.

[Mellon et al., 2000] Mellon, M. T., Jakosky, B. M., Kieffer, H. H., and Christensen, P. R. (2000). High resolution thermal inertia mapping from the Mars Global Surveyor Thermal Emission Spectrometer. *Icarus*, 148:437–455.

[Paige et al., 1994] Paige, D. A., Bachman, J. E., and Keegan, K. D. (1994). Thermal and albedo mapping of the polar regions of Mars using Viking thermal mapper observations, 1, North polar region. *J. Geophys. Res.*, 99:25959–25991.

[Paige and Keegan, 1994] Paige, D. A. and Keegan, K. D. (1994). Thermal and albedo mapping of the polar regions of Mars, 2, South polar region. *J. Geophys. Res.*, 99:25993–26013.

[Palluconi and Kieffer, 1981] Palluconi, F. D. and Kieffer, H. H. (1981). Thermal inertia mapping of Mars from 60^{o}S to 60^{o}N. *Icarus*, 45:415–426.

[Schofield et al., 1997] Schofield, J. T., Crisp, D., Barnes, J. R., Haberle, R. M., Magalhaães, J. A., Murphy, J. R., Seiff, A., Larsen, S., and Wilson, G. (1997). The Mars Pathfinder Atmospheric Structure Investigation/Meteorology (ASI/MET) experiment. *Science*, 278:1752–1757.

[Seiff and Kirk, 1977] Seiff, A. and Kirk, D. B. (1977). Structure of the atmosphere of Mars in summer mid-latitudes. *J. Geophys. Res.*, 82:4364–4378.

[Smith et al., 2001] Smith, M. D., Pearl, J. C., Conrath, B. J., and Christensen, P. R. (2001). Thermal Emission Spectrometer results: Mars atmospheric thermal structure and aerosol distribution. Journal of Geophysical Research, in press.